Journal of The Electrochemical Society, **153** (9) C641-C647 (2006) C641
0013-4651/2006/153(9)/C641/7/$20.00 © The Electrochemical Society

Precise Test of the Diffusion-Controlled Wet Isotropic Etching of Silicon via Circular Mask Openings

V. B. Svetovoy, J. W. Berenschot, and M. C. Elwenspoek

MESA† Research Institute, University of Twente, 7500 AE Enschede, The Netherlands

Isotropic etching of silicon in HF-based solutions is expected to be controlled by the diffusion of fluoride to the silicon surface. In order to gain quantitative understanding of the process, we studied etching of silicon in $HF/HNO_3/H_2O$ via circular mask openings and compared the results with the theoretical expectations. The cavity edges due to etching under the mask were analyzed with a high precision by processing the optical microscope images. Dependence on the etching time and opening size was investigated. A small anisotropy was observed in perfect agreement with the crystal orientation symmetry. A weak effect of free convection induced by the gravitation was resolved. Importance of careful temperature control is stressed. The observed time dependence agrees perfectly well with the theoretical prediction. It was verified with 1% precision. Dependence on the opening size predicted theoretically is not fully supported by the experiment. There is a small (4%) but clearly observable deviation from the theory. It is demonstrated that both time and opening size dependencies can be predicted with 1% precision if one introduces an effective diffusion "constant" that changes slightly with the opening size.
© 2006 The Electrochemical Society. [DOI: 10.1149/1.2217263] All rights reserved.

Manuscript submitted February 22, 2006; revised manuscript received April 27, 2006. Available electronically July 13, 2006.

Wet-chemical etching is a manufacturing technique, which is ideally suited for the machining of complicated small devices.[1] In this technique a mask is used to protect the material from the etchant, whereas the etching fluid dissolves the unprotected parts. The process is attractive for micromachining because, after the design of a proper mask, the production process is independent of the complexity of the design. In addition, the process is tension-free and the etched objects are free of burrs. These make wet-chemical etching an important technique in industry for the mass production of complicated objects with small features, such as shadow masks for color TV screens, lasers, printed circuit boards, filters, and sieves.

In this paper we are concentrating on the isotropic etching of silicon in $HF/HNO_3/H_2O$ solutions. An attractive feature of this technique is that etched shapes do not have sharp corners, which is important for a great number of liquid-handling devices, such as (bio)chemical analysis systems. Isotropic etching also helps to machine channels with varying diameter and neat bends, reaction chambers, and via holes, to name a few examples.

Crucial elements in the control of etching process are the proper design of a mask and the way the etching fluid is applied. In our case silicon nitride was deposited as the mask material in a low-pressure chemical vapor deposition process (LPCVD). The etched shapes are not identical to the mask, because etching also occurs under the mask edges. Diffusion of etching agent to the surface, forced or free convection of solution, local and global temperature distributions all can influence the process. These effects complicate mask design and, at the moment, there is no reliable design procedure available.

The first careful study of the isotropic etching of silicon without a mask in the system HF, HNO_3, and H_2O was described in a series of classical papers by Robbins and Schwartz.[2-5] It was established[2] that the etch rate is a function only of HF concentration when concentration of HNO_3 is high. The reaction proceeds by an oxidation step followed by the dissolution of the oxide. The dissolution step is rate limiting at high HNO_3 concentration. The authors argued that the flow of reagent to the surface by diffusion determines the etch rate. It means that the surface reactions proceed fast in comparison with the supply of active components. Investigation of the temperature dependence of the process[4] gave additional support to this point of view. More recent studies showed that mass-transfer effects are quite significant in acid etching[6-9] and identification of the rate-controlling step becomes more critical than the knowledge of the actual chemistry.[10] The shift in the limiting step, from kinetics to diffusion, in etching of thermal oxide by HF was discussed.[11] Monk et al. also reviewed the chemical reaction mechanism and kinetics of silicon oxide etching.[12]

Qualitative understanding of the etching process was used for applied researches,[13-16] but for precise design of masks we need much more detailed information on the process. Quantitative investigation of the diffusion-controlled isotropic etching via a mask opening has never been done. We consider this work as a first step toward a controllable isotropic etching. It is reasonable to start with very simple structures, which can be relatively easy to model theoretically. The isotropic etching in the diffusion-controlled regime was investigated theoretically for circular[17] and slitlike[18] openings in the mask. The diffusion equation was solved at specified boundary conditions and definite analytic solutions were found in the limits of shallow and deep cavities. The effects of free convection and local temperature distribution were neglected, but forced convection has been tackled numerically in a number of studies.[19-22]

For the first experimental test of the diffusion-controlled etching we chose the etching via circular mask openings. In contrast with etching via slits, in this case it is possible to analyze small anisotropy, which inevitably is present in realistic systems. The etch times and diameter of holes in the mask were chosen in the range where theoretical predictions are available in the analytic form.

Theory

Isotropic etching through a round aperture in a mask was considered in Ref. 17. The diffusion equation

$$\partial c/\partial t = D\nabla^2 c \quad [1]$$

for the concentration of the active etching component c (mol/m^3) with the diffusion coefficient D was solved assuming a diffusion-controlled process. This means that the reaction on the surface proceeds fast in comparison with the diffusion, and for this reason the boundary condition on the etched surface is

$$c = 0 \quad [2]$$

while on the mask the nonpenetration condition is realized

$$\partial c/\partial n = 0 \quad [3]$$

where n is the direction normal to the mask. Far away from the surface c must be equal to the concentration in the solution c_0, and at the initial moment $t = 0$ the concentration is everywhere equal to c_0. Because the etched surface is moving, its position is an unknown of the problem. That is why an additional boundary condition is needed. This condition follows from equality of the flux of dissolved material $c_{Si}v$ to the flux of the active component reacting with silicon $k_a\mathbf{J}_a$. Here, c_{Si} is the silicon concentration, v is the etch rate, $\mathbf{J}_a = -D\nabla c$ is the flux of the active component impinging on the surface in the diffusion-controlled regime, and k_a is the probability for an impinging particle (molecule, atom, or ion) to stick to the surface with the following interaction with one Si atom in any chemical form. The value $1 - k_a$ can be interpreted as the reflection

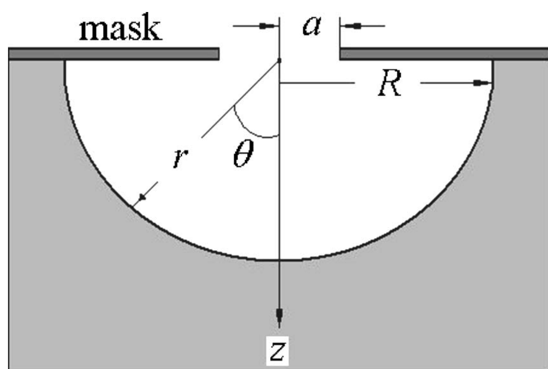

Figure 1. The cross section of the etched structure. Main characteristics of the cavity and opening in the mask are indicated.

coefficient. Therefore, the additional condition on the etched surface is the following

$$v = -(k_a D/c_{Si})\,\nabla c \quad [4]$$

If the function $f(t,x,y,z) = 0$ describes the etched profile, then the evolution of this profile is given by the equation

$$\partial f/\partial t + v \cdot \nabla f = 0 \quad [5]$$

For analysis of the problem it is important to introduce dimensionless variables and parameters

$$\tau = Dt/a^2, \quad X = x/a, \quad Y = y/a, \quad Z = z/a,$$

$$C = c/c_0, \quad \beta = c_{Si}/k_a c_0 \quad [6]$$

where a is the radius of circular opening in the mask. In the dimensionless form the problem is characterized by the only parameter β. It can be understood[23] as the ratio of volume which reacting active particle occupies in the solution, to that which silicon atom occupies in the solid. Obviously this parameter is naturally large.

The analytic solutions of the problem 1-5 can be found in two limit cases[17]: for shallow cavities when the dimensionless time τ is in the range

$$1 \ll \tau \ll \beta \quad [7]$$

and for deep cavities when

$$\tau \gg \beta \quad [8]$$

In this study we consider the case of deep cavities. Taking as typical parameters $D \sim 10^{-9}$ m^2/s,[24] $a \sim 10$ μm, and $\beta \sim 100$, one finds from Eq. 6 and 8 that the etch time t should be much larger than 10 s. This condition is met in any realistic etching process. In this asymptotic regime the diffusion field can be considered as quasi-stationary. Evolution with time happens due to slow development of the etched profile according to Eq. 5. In the spherical coordinates (r,ϑ) the etched profile is described by the function

$$r^2 = R^2(R^2 - a^2)/(R^2 - a^2 \sin^2 \vartheta) \quad [9]$$

where $R = R(\tau)$ is the underetch radius (see Fig. 1) defined as

$$R = a\sqrt{1 + (3\tau/\pi\beta)^{2/3}} \quad [10]$$

Although τ/β is large we cannot completely neglect a in comparison with R in the range of experimentally investigated sizes (a = 6–40 μm) and etch times (t = 10–120 min), but for all practical purposes it is sufficient to keep only the first correction $\sim a/R$. With this precision the cavity shape is given by the equation

$$r(\vartheta) \approx a(3\tau/\pi\beta)^{1/3}[1 + (3\tau/\pi\beta)^{-2/3}\sin^2 \vartheta/2] \quad [11]$$

The underetch radius is defined from here as $R = r(\pi/2)$. Equations 10 and 11 are the main theoretical results, which will be used for comparison with the experiment. The shape of the cavity is defined by the only parameter D/β; dependence on the etching time t, mask opening size a, and spherical angle ϑ is completely defined.

The model described above does not take into account the free convection, local heating around a cavity, diffusion of the reaction products, and inevitable anisotropy of the etching. Any of these effects can influence the etching process and the experiment can answer the question how significant this influence is.

Experimental

Sample preparation and processing.— Silicon wafers with the orientations (100), (110), and (111) were analyzed. The wafers were p-type doped with a resistivity of 5–10 Ω cm. An additional set of highly doped (0.0015–0.0019 Ω cm) wafers with (100) orientation was also studied. All the wafers had a diameter of 100 mm and were doped with boron. Standard cleaning procedures and removal of native oxide were followed by the deposition of 500 nm thick low-stress silicon-rich nitride (SiRN) obtained by LPCVD process. Both sides of the wafers were covered with nitride. Standard photolithography was done with Oline 907-17 photoresist. Dry etching of SiRN was carried out with RIE-Elektrotech Twin system PF340. Each wafer was diced to four quarters with the dicing lines perpendicular and parallel to the primary flat. Finally the photoresist was striped off in 100% HNO_3.

The mask pattern on the front side of all pieces of the wafers was identical and consisted of holes in SiN mask with the diameters from 12 to 80 μm with an increment of 4 μm. The identical sets of holes were located in different places on a quarter wafer. The holes were positioned far enough from each other to exclude mutual influence during the etching process. The back side of each piece but one was protected by nitride to prevent the back-side etching. The open area on the front side was negligible to give any influence on the global temperature during the etching.

The etching solution contained 1 part (volume) of HF (50%), 6 parts of HNO_3 (69%), and 2 parts of deionized water. The solution was prepared in a beaker and kept at least 1 h in the fume hood before starting the etching process. This delay was important to guarantee that all samples were etched at the same temperature. One liter of the solution was used to etch all eight wafers at room temperature, $T_0 = 22$°C. Four pieces of different wafers [low-doped (100), (110), (111), and highly doped (100)] were etched at a time in the vertical position. The pieces were fixed in a Teflon holder, which was placed gently in the beaker with the solution. No agitation of the solution was undertaken during the etching process. The etch times were 10, 21, 30, 45, 63, 82, 100, and 120 min; a typical etch rate was of about 1 μm/min. After the process standard rinsing and drying were done.

Data collection.— The cavity shape in the asymptotic regime $\tau/\beta \gg 1$ is nearly spherical, as it follows from Eq. 11. The shape cannot be checked in this experiment due to the presence of small anisotropy, which can be easily confused with the effect. The most convenient characteristic of the cavity that can be precisely analyzed experimentally is the underetch radius R. Because the nitride mask is transparent for visible light, the edges of the cavities were clearly visible with the optical microscope (see Fig. 2). The resolution of the optical images was 0.134 μm/pixel while $2R < 150$ μm and 0.334 μm/pixel for larger R. The edge of a cavity could be resolved within a few pixels. Optical images of individual cavities were recorded and analyzed. In all, more than 500 images were processed. Each image was filtered to remove small spots and tracked for the edges of the mask opening (circle) and the cavity (noncircular shape). In this way the digital data were collected for the underetch radius $R(\varphi)$ as a function of the polar angle φ in (100), (110), and (111) planes for all opening sizes and etching times. Typical results are presented in Fig. 2. The photos in the top row were taken for an etch time of 21 min and an opening radius of 18 μm. The graphs in the bottom row are the digital data for $R(\varphi)$ extracted from these photos. Digital data for the mask opening $a(\varphi)$ were collected only

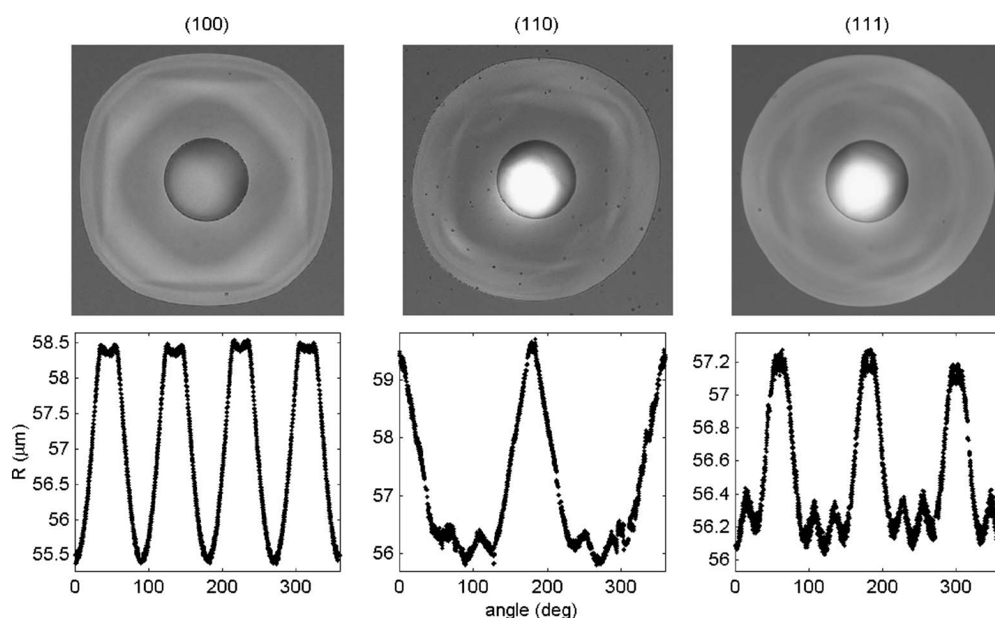

Figure 2. (top row) Optical microscope images of the cavities etched for 21 min with a mask opening radius of 18 μm in samples with orientations (100), (110), and (111). Anisotropy due to wafer orientation is clearly seen. (bottom row) Digitized data extracted from the images for the underetch radius $R(\varphi)$ as a function of in-plane polar angle φ. The graphs show that the observed anisotropy is in a perfect agreement with the in-plane symmetry transformations: 4-fold, 2-fold, and 3-fold for (100), (110), and (111), respectively. Very small deviations from these symmetries demonstrate high level of precision in our data. The magnitude of anisotropy is significantly smaller for the (111) sample.

for part of the images. This is because significant reflection from the bottom of the cavity in some cases spoiled the central part of the image.

Precision of the data.— Although the etching in $HF/HNO_3/H_2O$ is considered isotropic, we see well-observable anisotropy for all kinds of wafers. Detailed investigation of the anisotropy will be given elsewhere. Here, the observed anisotropy is in a perfect agreement with the in-plane symmetry transformations of Si crystal. These symmetries are 4-fold, 2-fold, and 3-fold rotations for (100), (110), and (111) wafers, respectively. Additional reflection transformations allow only even functions of the in-plane angle φ. It means that the underetch radius for each wafer orientation can be presented as cosine Fourier series

$$R^{(m)}(\varphi) = R_0^{(m)} + \sum_{n=1}^{\infty} R_n^{(m)}\cos(mn\varphi) \quad m = 4,2,3 \qquad [12]$$

where $m = 4$, 2, and 3 correspond to (100), (110), and (111) wafers, respectively. We found that four-parametric fits with Eq. 12 describe all the cavities very well with higher harmonics to be on the noise level. No systematic deviations from the symmetry predictions were noted. An example of the fit is presented in Fig. 3 for the (100) sample shown in Fig. 2. Only 10% of the data are shown for clarity.

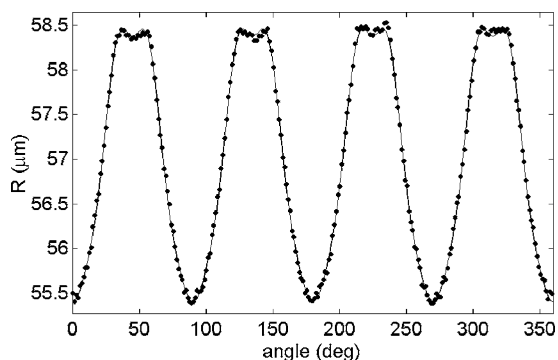

Figure 3. Four-parameters fit (solid line) of the data in Fig. 2 for (100) wafer ($m = 4$). Only 10% of the data (dots) are shown for clarity. The figure demonstrates an excellent agreement of the observed in-plane cavity shape with the symmetry restrictions due to the crystal orientation.

The model described in the previous section deals only with the isotropic etching. To make the comparison with the theoretical predictions, we can analyze the isotropic part of the expansion 12, which is presented by the first term

$$R_0(t,a) = \frac{1}{2\pi}\int_0^{2\pi} R(\varphi;t,a)d\varphi \qquad [13]$$

It is the averaged underetch radius considered as a function of the etching time t and opening radius a. It can be extracted from the data with very high precision. Typical root-mean-square (rms) errors in the radius are of 0.5 pixels or 0.07 and 0.15 μm for larger and smaller magnifications, respectively. The relative errors in the radius for both magnifications are estimated as 0.3%. This high level of precision is explained by good quality of images and significant amount of the data collected from each image (1500–2500 points).

One could imagine some systematic effects which can influence the cavity shape, such as free convection due to vertical positioning of the samples or inhomogeneous temperature distribution around a cavity. For example, the convection should break the symmetry due to preferential direction in the etchant flow but it never was observed in our experiment. What we did observe was the influence of convection on the displacement of the cavity center relative to the opening center, as shown in Fig. 4. The figure gives displacement (a) and direction (b) of this displacement as functions of the opening size for (100), (110), and (111) samples etched together for 30 min. The displacements for all samples are in agreement with each other, increases with a, and exceeds the measurement errors for $a \geqslant 18$ μm. The direction of the displacement is scattered, while the displacement cannot be resolved within the errors but converges reasonably well to the direction of gravitational field (approximately 45°) for $a \geqslant 18$ μm. A maximal displacement of 7 μm was observed for the longest etching time $t = 120$ min and the largest opening size $a = 40$ μm.

All our data for the shape of the cavities are in perfect agreement with the wafer symmetries. This means that the convection drives a cavity as a whole but does not influence its shape. Of course, we can make this statement only for the top view but not for three-dimensional shape of cavities. We have no clear explanation for this effect at the moment but it simplifies our analysis because one can neglect the convection in the investigation of the underetch radius.

The holes in the nitride mask are reproducible with a nominal precision of 1 μm (in shape and in size) due to restrictions in the fabrication of masks for lithography. For the samples etched for 10,

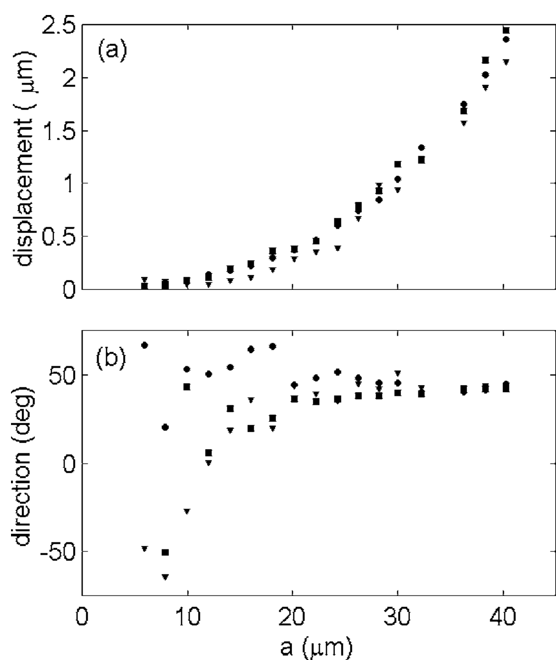

Figure 4. Displacement of the cavity center relative to the center of the mask opening induced presumably by the free convection in the gravitational field. The data correspond to the samples of different crystallographic orientation etched together during 30 min. Circles, squares, and triangles represent (100), (110), and (111) samples, respectively. (a) Absolute value of the displacement; it exceeds the measurement errors for $a \geqslant 18$ μm. (b) Direction of the displacement; it is in agreement with the direction of the gravitational field for $a \geqslant 18$ μm.

30, and 63 min we collected the data on actual shapes and sizes of the holes in the nitride mask. It was found that the largest rms deviation from the circular shape was 0.2 μm but the radius of holes deviates more significantly from the nominal size. Figure 5 shows the difference between the measured radius a_m and nominal radius of the hole a as a function of a. The samples of different orientations were etched for 30 min. The figure demonstrates a general tendency: the measured radius is larger than the nominal; the difference increases with a reaching its maximal value of 1 μm at largest a. However, one cannot conclude that there is any dependence on the

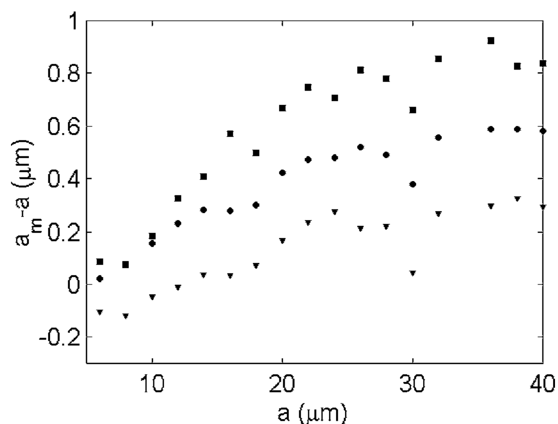

Figure 5. The difference between the measured radius of the mask hole a_m and the nominal radius a as a function of a. The samples with the orientations (100) (circles), (110) (squares), and (111) (triangles) were etched together for 30 min. The figure demonstrates that, in general, the observed radius is larger then the nominal one and deviation increases with a.

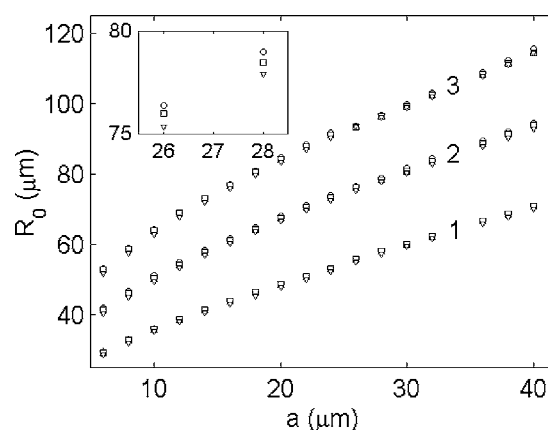

Figure 6. Dependence of the underetch radius R_0 on the radius of mask opening a. Series of points marked as 1, 2, 3 correspond to the samples etched for 10, 30, and 63 min, respectively. Samples of different orientation are presented by open circles (100), squares (110), and triangles (111). They hardly can be resolved on the scale of this figure. Inset shows details for two values of a = 26 and 28 μm corresponding to t = 30 min.

orientation because different relations between (100), (110), and (111) samples were observed for the etching times 10 and 63 min.

There are too many effects which can contribute to indefiniteness of the hole sizes to make any conclusion on the origin of the deviations: lithography mask errors, inhomogeneity of the plasma etching of mask or variation of the etching time, slow wet etching of the mask, and others. In what follows we use the nominal size of the holes. The relative error in R, which is introduced in this way, can be estimated as $\Delta R/R \approx \Delta a/3a$ (see Eq. 10). It is on the level of 1%. A similar error of 1% appears due to indefiniteness of the etching time, which is estimated as Δt = 30 s.

Results

Typical results for the underetch radius $R_0(a)$ as a function of the opening radius are presented in Fig. 6 for three different etching times. The samples with different crystal orientations give very close results, which cannot be resolved on the scale of the figure. The difference between (100), (110), and (111) samples is just a little bit larger than the level of errors but it is systematic. The underetch radius is the largest for (100) and the smallest for (111) samples. We did not observe significant deviations between low and highly doped (100) samples. A very small difference was found between cavities etched in the center and in the periphery of the same sample. One (110) sample had no SiN protecting mask on the back side, so that the cavities and the back side were etched simultaneously. One can expect that the heat produced on the back side due to the significant area which is etched will influence the cavity etching. This is indeed the case as Fig. 7 demonstrates. This figure gives a comparison of the (110) samples with protected and open back sides etched for 21 min. The sample with open back side is etched faster. Additionally, we observed that the change in the solution temperature of about of 2°C has significant influence on the cavity sizes. All that shows that the small variation of the temperature is an important factor which cannot be neglected.

Comparison between theory and experiment.— The main prediction of the theory is that the ratio R_0/a does not depend on t and a separately but only in the combination t/a^2. According to Eq. 10 this dependence can be presented as

$$[(R_0/a)^2 - 1]^{3/2} = (3D/\pi\beta) \cdot t/a^2 \qquad [14]$$

Log-log plot of the data for (100) samples is shown in Fig. 8a. One can see that all the points are attracted to one line. It gives strong support to the theoretical prediction. Moreover, according to Eq. 14 this line must be a straight line with the slope equal to 1. The best

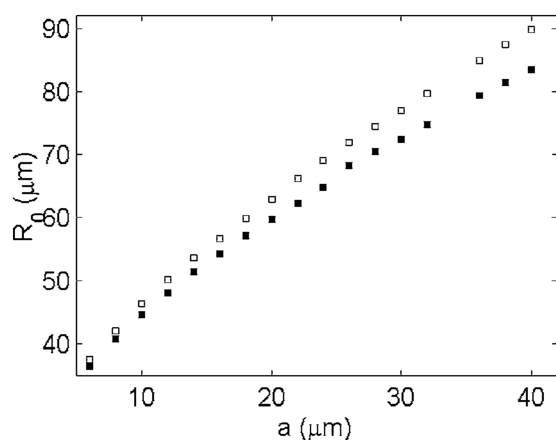

Figure 7. Comparison of two (110) samples etched together for 21 min. Open squares correspond to the sample with open back side. The heat produced in the reaction with the back side heats up the wafer so that the cavities on the front side are etched faster. Solid squares present the sample with protected back side.

straight line fitting the data is $0.96 \ln(t/a^2) + 6.02$. The slope is really close to 1 and the free term 6.02 can be used to estimate the unknown parameter D/β from the relation $\ln(3D/\pi\beta) = 6.02$. We have found $D/\beta \approx 430\ \mu m^2/min = 7.2 \times 10^{-12}\ m^2/s$. This value is in good correspondence with our expectations for the parameters $D \sim 10^{-9}$–$10^{-10}\ m^2/s$ and $\beta \sim 100$. Similar behavior of the data was found for the samples with (110) and (111) orientation.

The high precision of our data allows the separation of an effect which is not described by the theory. As one can see in Fig. 8a the dots lie perfectly on the straight line for small and large values of

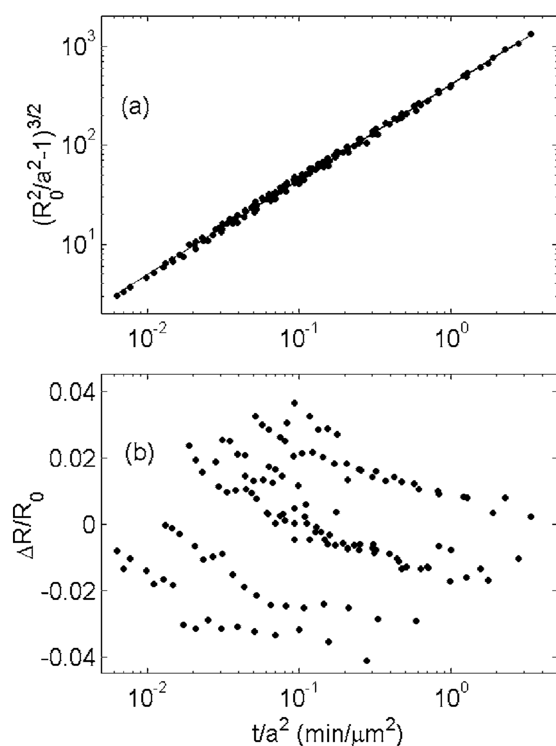

Figure 8. (a) All the data for (100) samples plotted against only one variable t/a^2 (dots). A straight line, which fits the data, gives strong support to the theoretical model of the diffusion-controlled etching. (b) Relative deviation between the data and the fitting line in (a). The points are not arbitrarily scattered, which indicates a systematic effect in the data on the level of 4%.

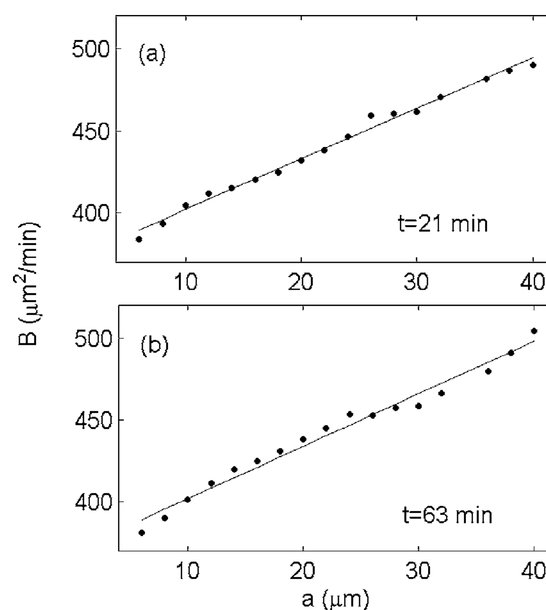

Figure 9. Values of the parameter B (dots) calculated with Eq. 15 for two etching times: (a) $t = 21$ min; (b) $t = 63$ min. The data demonstrate that B is not just a constant as predicted in the simplest variant of the model but a linear function of a. The solid lines present the linear fit of the data.

t/a^2, but in the middle of the interval the dots are scattered more significantly. The relative deviation of the data from the straight line is shown in Fig. 8b. One can see that the magnitude of the deviations is 4% but the points are not scattered arbitrarily and there must be some systematic effect that is not taken into account by Eq. 14.

To see this effect more clearly we construct a parameter B as

$$B = (a^2/t)(R_0^2/a^2 - 1)^{3/2} \qquad [15]$$

According to the original model[17] this parameter should be a constant equal to $3D/\pi\beta$. To check this prediction we plotted B as a function of a for fixed etching time. For $t = 21$ and 63 min the values of B for (100) samples are presented in Fig. 9 by the points. One can see that B agrees much better with a linear function of a than with a constant. For each t the values of B were fitted with the linear dependence

$$B(a) = B_1 + B_2 a \qquad [16]$$

The parameters B_1 and B_2 found for different etching times do not show any statistically significant time dependence, and for this reason they can be characterized by their mean values and variances. For (100) samples we have found

$$(100): \quad B_1 = 377 \pm 11\ \mu m^2/min, \quad B_2 = 3.3 \pm 0.3\ \mu m/min \qquad [17]$$

Using the parameters 17 one can predict the time behavior of the underetch radius according to Eq. 15. The experimental data for the opening sizes $a = 12$, 20, 28 μm are compared with the prediction of the model in Fig. 10. Note that the time dependence is predicted without adjustable parameters. The rms deviations between the experimental $R_0(t)$ and the model predictions are 0.65, 0.8, 1.1 μm for $a = 12$, 20, 28 μm, respectively. In the relative values the agreement is better than 1%.

The level of agreement between the theory and experiment can also be characterized by the rms deviation for all the data (136 points). In this case the theoretical prediction is made with two adjustable parameters B_1 and B_2. Using the parameters given by 17 we have found for the relative rms deviation of $R_0(t,a)$

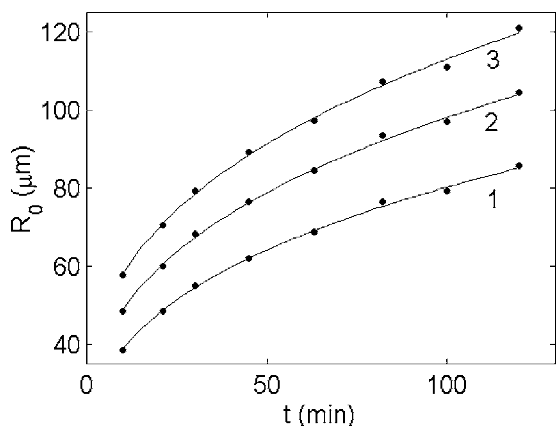

Figure 10. Comparison between experiment and model prediction of the time dependence of the underetch radius without adjustable parameters. The dots present experimental data for $a = 12$, 20, 28 µm marked 1, 2, and 3, respectively. The solid curves are the corresponding theoretical predictions. Agreement between the theory and experiment is better than 1%.

$$\Delta R_0/R_0 = 0.9\% \qquad [18]$$

This level of agreement is in good correspondence with our expectations for the experimental errors $\Delta R_0/R_0 \approx 1\%$ due to uncertainties in a and t. Coincidence between these two figures ensures that there are no other sources of significant errors in our data.

Similar analysis was done for (110) and (111) samples. In these cases we have found

$$(110): \quad B_1 = 368 \pm 8 \ \mu\text{m}^2/\text{min} \quad B_2 = 3.4 \pm 0.4 \ \mu\text{m/min}$$
$$\Delta R_0/R_0 = 0.9\% \qquad [19]$$

$$(111): \quad B_1 = 346.5 \pm 9 \ \mu\text{m}^2/\text{min} \quad B_2 = 3.5 \pm 0.4 \ \mu\text{m/min}$$
$$\Delta R_0/R_0 = 0.75\% \qquad [20]$$

Comparison of these results with that for (100) samples shows that one cannot distinguish the experimental errors between (100) and (110) samples. In the sense of isotropic etching they behave similarly. For (111) samples the parameter B_1 is a little bit smaller. It can be explained by slightly different constant k_a for (111) wafer. However, this difference should not be taken very seriously because the difference is within 2 standard deviations.

Discussion

One of the findings of this study is the relation of the observed anisotropy with the in-plane symmetry of the wafer. It seems obvious but the precision of 0.5% with which this relation holds true in the experiment is amazing. Of course, the symmetry should be broken by the convection, but we did not observe any statistically significant deviations. To all appearances this is because in our experiment there was no forced convection. The free convection induced by the change of the solution density due to formation of the reaction products is a very weak effect as Fig. 4 shows. For this reason the underetch size evolves much faster than the convection drags the cavity.

Undoubtedly the diffusion theory gives a good prediction for the etching process as Fig. 8a demonstrates. The observed time dependences of the underetch radius is fully confirmed by the experiment. However, the prediction of the dependence on the opening size a is not completely supported by our data. The parameter B in Eq. 15 is presented much better by a linear function of a than by a constant as the theory predicts. Effectively it means that the physical parameter D/β depends on the opening size

$$(100): \quad (D/\beta)_{\text{eff}} \approx 395 + 3.5a \ \mu\text{m}^2/\text{min} \qquad [21]$$

Although the linear in a term is not a principal part of the parameter, its contribution to $(D/\beta)_{\text{eff}}$ is observable and far exceeds the experimental errors.

What is the physical reason for this dependence on a? We do not believe that it has something to do with the free convection just because B changes significantly, but the free convection is a minor effect. Importance of the free convection can be checked experimentally by positioning the samples horizontally. Observation of the time dependence in accordance with the expectation significantly restricts possible physical modifications of the process. For example, in the model it was assumed that the diffusion completely controls the etching. One could relax this condition and assume that the reaction on the surface is not infinitely fast. In this case the boundary condition on the surface instead of 2 will be

$$-D(\partial c/\partial n) = k_r c \qquad [22]$$

where k_r is the reaction rate (m/s). In the dimensionless form the normal coordinate n is scaled as n/a and the finite reaction rate can appear in the problem via the dimensionless parameter $D/k_r a$. Because this parameter has to be small in our case it can appear in the expression for R_0 as a linear correction

$$R_0/a = (3\tau/\pi\beta)^{1/3} + (D/k_r a) f(\tau/\beta), \quad \tau/\beta \gg 1, \quad D/k_r a \ll 1 \qquad [23]$$

where $f(\tau/\beta)$ is an unknown function. The time dependence $\sim t^{1/3}$ will not be disturbed if $f(\tau/\beta) \sim (\tau/\beta)^{1/3}$. Equation 23 can be presented in the form similar to 15

$$R_0/a = [B(a)\tau/\beta]^{1/3} \qquad [24]$$

but in contrast with 16 $B(a)$ is not a linear function of a but $B(a) = B_1 + B_2/a$. This dependence is not supported by our data because B is not decreased with a.

As the other modification of the model we took the reaction product into consideration. We analyzed situations when removal of the reaction product from the cavity is controlled by the desorption from the surface or by the diffusion of the product in the solution. In both cases the time dependence of the etching process is not supported by the observations. We need to look for a mechanism responsible for the dependence of the diffusion constant D or parameter $\beta = c_{\text{Si}}/k_a c_0$ on the opening size a.

One possibility is the local temperature rise around a cavity. From Eq. 11 it follows that the cavity is nearly spherical and, neglecting the correction of the order of a/R for the total volume etched out, one finds

$$V \approx 2a^3(\tau/\beta) = 2(D/\beta)at \qquad [25]$$

The volume depends linearly on both t and a. Because the reaction with silicon is exothermic, it means that the cavity is a local heat source of a constant power. This power increases linearly with the opening size. The constant power source will produce a stationary local temperature distribution around the cavity. The etching is going on at the maximum of this distribution, where the surface temperature T_s is a little bit higher than the surrounding temperature T_0. The dependence of the process on the temperature originates from the parameter D/β, which is expected to have ordinary activation energy behavior[4]

$$D/\beta \sim \exp(-E_a/kT_s) \qquad [26]$$

where E_a is the activation energy and k is the Boltzmann constant. The observed effect will be explained if T_s does not depend on t and its value is sufficiently large in comparison with T_0.

We can estimate T_s considering the boundary condition of the heat production on the etched surface. This condition connects the jump of the heat flux on the surface of the cavity with the heat of the reaction

$$\lambda_1(\partial T_1/\partial n) - \lambda_2(\partial T_2/\partial n) = Q_s \quad [27]$$

where the index $i = 1,2$ refers to silicon or solution, λ is the heat conductivity of the material, n is the direction normal to the cavity surface, and Q_s is the surface source of the heat. This source is given by the flux of active particles, k_aJ_a, multiplied by the enthalpy of the reaction H_0

$$Q_s = -H_0k_aD(\partial c/\partial n) \approx (H_0c_{\mathrm{Si}}a/\pi R^2)(D/\beta) \quad [28]$$

Because the heat conductivity for Si is much larger than that for the solution ($\lambda_1 \gg \lambda_2$), the heat produced in the reaction propagates mostly in silicon. The temperature gradient on the surface can be estimated as $\partial T_1/\partial n \sim T_s/R$. Using 27 and 28, one finds an estimate for the surface temperature

$$T_s \sim (H_0c_{\mathrm{Si}}/\pi k_1)(a/R)(D/\beta) \quad [29]$$

The first conclusion which can be drawn from Eq. 29 is that the temperature is proportional not just at the opening size but also the ratio a/R. This ratio is a function of t due to time dependence of the underetch radius R. Moreover, the magnitude of the temperature rise is a few orders of magnitude smaller than needed for the explanation of the effect.

To understand linear dependence of the parameter B on the opening size, additional experimental investigation is needed, such as which physical parameters influence B_2 in Eq. 16. One should analyze the dependence of this parameter on the surrounding temperature and on the composition of the solution. It is also helpful to see if the same effect exists in the etching of slits, where reliable theoretical predictions are also available.[18]

Conclusions

In this paper we tried to answer the question how well we understand the process of isotropic silicon etching in $HF/HNO_3/H_2O$ solutions. The theory assumes that the etching process is controlled by the diffusion of the active component to the surface. Holes in the mask were chosen as the simplest structure for investigation. In the experiment the cavities were investigated as a function of the etching time t and the mask opening radius a. It was possible to make unambiguous conclusions due to high precision of our measurements. The in-plane shape of the cavities was recorded with relative precision better than 0.5%. In reality the isotropic etching of a single crystal demonstrated some level of anisotropy. Wafers of different orientations were investigated and it was established that the anisotropy is completely controlled by the in-plane symmetry of the crystal. This symmetry gave us an independent way to check the precision of the data.

Influence of the free convection induced by the gravitational field was observed as a small displacement of the cavity center in respect to the mask opening. Surprisingly, the convection did not break the crystal symmetry within the experimental errors. We observed that even a small change in the solution temperature to 1–2°C influenced the underetch size markedly. One can conclude that the temperature control is crucial for reproducibility of the process. Local heating due to exothermicity of the reaction happens to be negligible if the etched area is small. We also did not observe that the doping level played any role for p-type silicon.

The theory predicts that in the asymptotic regime when the dimensionless time is large, $\tau \gg \beta$, the ratio R_0/a is a function of only t/a^2 but not two separate variables t and a. The experiment proved with a precision of 4% that this is indeed the case. However, the precision of our data was considerably better and some additional systematic effect, which is not described by the simple diffusion model, was noted. The original theoretical model explained perfectly well the time dependence of the etching process. But, it was only partially successful for the explanation of the dependence on the opening size a. To all appearances, the detailed explanation of a dependence should include some new physics.

University of Twente assisted in meeting the publication costs of this article.

References

1. M. C. Elwenspoek and H. Jansen, *Silicon Micromachining* (Cambridge University Press, Cambridge (1998).
2. H. Robbins and B. Schwartz, *J. Electrochem. Soc.*, **106**, 505 (1959).
3. H. Robbins and B. Schwartz, *J. Electrochem. Soc.*, **107**, 108 (1960).
4. B. Schwartz and H. Robbins, *J. Electrochem. Soc.*, **108**, 365 (1961).
5. B. Schwartz and H. Robbins, *J. Electrochem. Soc.*, **123**, 1903 (1976).
6. K. S. Nahm, Y. H. Seo, and H. J. Lee, *J. Appl. Phys.*, **81**, 2418 (1997).
7. R. W. Fathauer, T. George, A. Ksendzov, and R. P. Vasquez, *Appl. Phys. Lett.*, **60**, 995 (1992).
8. K. McAndrews and P. Sukanek, *J. Electrochem. Soc.*, **138**, 863 (1991).
9. J. P. John and J. McDonald, *J. Electrochem. Soc.*, **140**, 2622 (1993).
10. M. S. Kulkarni and H. F. Erk, *J. Electrochem. Soc.*, **147**, 176 (2000).
11. D. J. Monk, D. S. Soane, and R. T. Howe, *J. Electrochem. Soc.*, **141**, 264 (1994);, **141**, 270 (1994).
12. D. J. Monk, D. S. Soane, and R. T. Howe, *Thin Solid Films*, **232**, 1 (1993).
13. R. W. Tjerkstra, M. de Boer, J. W. Berenschot, J. G. E. Gardeniers, A. van den Berg, and M. C. Elwenspoek, *Electrochim. Acta*, **42**, 3399 (1997).
14. C.-T. Seo, C.-H. Bae, D.-S. Eun, J.-K. Shin, and J.-H. Lee, *Jpn. J. Appl. Phys., Part 1*, **43**, 7773 (2004).
15. Y. Wang, C. Zhu, Y. Li, and C. Wua, *Electrochem. Solid-State Lett.*, **7**, C104 (2004).
16. R. W. Tjerkstra, Ph.D. Thesis, University of Twente (1999).
17. H. K. Kuiken, *J. Eng. Math.*, **45**, 75 (2003).
18. H. K. Kuiken, *Proc. R. Soc. London*, **A396**, 95 (1984).
19. C. B. Shin and D. J. Economou, *J. Electrochem. Soc.*, **138**, 527 (1991).
20. C. H. Driesen, J. G. M. Kuerten, and M. Streng, *J. Eng. Math.*, **34**, 3 (1998).
21. C. H. Driesen and J. G. M. Kuerten, *Comput. Mech.*, **25**, 501 (2000).
22. C. H. Driesen,Ph.D. Thesis, University of Twente (1999).
23. H. K. Kuiken, J. J. Kelly, and H. L. Notten, *J. Electrochem. Soc.*, **133**, 1217 (1986).
24. D. R. Lide, *Handbook of Chemistry and Physics*, 74th ed., pp. 5–91, CRC Press, Boca Raton, FL (1993).